Spin Label EPR-Based Characterization of Biosystem Complexity

Janez Štrancar,*,† Tilen Koklič,† Zoran Arsov,† Bogdan Filipič,‡ David Stopar,§ and Marcus A. Hemminga||

Laboratory of Biophysics, "Jožef Stefan" Institute, Jamova 39, SI-1000 Ljubljana, Slovenia, Department of Intelligent Systems, "Jožef Stefan" Institute, Jamova 39, SI-1000 Ljubljana, Slovenia, Biotechnical Faculty, University of Ljubljana, Večna pot 111, SI-1000 Ljubljana, Slovenia, and Laboratory of Biophysics, Wageningen University, Dreijenlaan 3, NL-6703 HA Wageningen, The Netherlands

Received August 13, 2004

Following the widely spread EPR spin-label applications for biosystem characterization, a novel approach is proposed for EPR-based characterization of biosystem complexity. Hereto a computational method based on a hybrid evolutionary optimization (HEO) is introduced. The enormous volume of information obtained from multiple HEO runs is reduced with a novel so-called GHOST condensation method for automatic detection of the degree of system complexity through the construction of two-dimensional solution distributions. The GHOST method shows the ability of automatic quantitative characterization of groups of solutions, e.g. the determination of average spectral parameters and group contributions. The application of the GHOST condensation algorithm is demonstrated on four synthetic examples of different complexity and applied to two physiologically relevant examples − the determination of domains in biomembranes (lateral heterogeneity) and the study of the low-resolution structure of membrane proteins.

INTRODUCTION

Spectroscopic techniques are widely applied to obtain relevant information about the structure and dynamics of biological systems in a nondestructive way. Electron paramagnetic resonance (EPR) spin labeling is particularly suitable for studying properties of biological membranes, since it is able to provide detailed information about structural and dynamic properties of lipids and membrane proteins, e.g. restrictions of rotational motions, rate of rotational motions, location relative to the water and oxygen profile in membranes, and local polarity.

Biological membranes are composed of many different components and coexisting phases.[1−3] It turns out that even simple model membranes composed of only two chemical species of lipids show a lateral phase separation and domain formation giving rise to detection of a coexistence of different rotational motions as well as polarities of the molecules in membranes. EPR membrane spectroscopy is based on the introduction of lipophilic spin probe molecules into biomembranes. Through EPR spectral line shapes the spin probes report about the number of different local rotational motions and polarities as well as the characteristics of each rotational motion and polarity. The number of the reported motional patterns can be 1 in biochemically pure system at a temperature where the membrane would be in fluid state − "1 solution" in Figure 1. If a membrane would consist of more than one constituent, we could find two or more sharply defined solutions with different motional characteristics and polarities − "2 solutions" and "several discrete solutions"

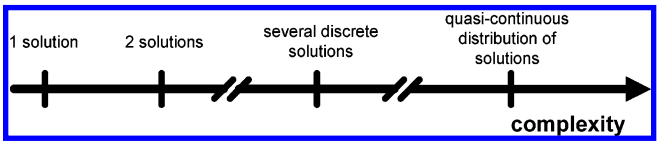

Figure 1. Schematic representation of biosystem complexity.

in Figure 1. In this case we would describe the complexity of the membrane system as low. However, when a membrane has many different constituents, as is the case of real biological membranes, the rotational motions and polarity can vary a lot in the lateral direction and so a large number of different solutions could be obtained. In general, the restrictions of motions, the rate of motion and polarity could continuously change among different solutions − "quasi-continuous distribution of solutions" in Figure 1. In such a case we would say that the complexity of the membrane system is high.[4−6]

Regarding the actual complexity of lipid composition and biophysical interactions in biological membranes it is therefore not a surprise that spin label EPR spectra of such systems are composed of several superimposed spectral components. However, a common spectroscopic approach in dealing with such a complex EPR spectra is to fit them with a limited number of discrete spectral components. In many methods, it is assumed that the number of components is two[7,8] or few.[9,10] But in the biosystems with high complexity this number of components can still not sufficiently describe the system.

In addition to membrane domain studies, recently site-directed spin labeling (SDSL) EPR was shown to be useful for studying structural dynamics of membrane proteins.[11−13] When the conformation of a protein is changed, the motional characteristics of a spin label that is attached to the protein are likely to change. This is again related to the anisotropy

* Corresponding author phone: +386 1 477 32 26; fax: +386 1 426 32 69; e-mail: janez.strancar@ijs.si.
† Laboratory of Biophysics, "Jožef Stefan" Institute.
‡ Department of Intelligent Systems, "Jožef Stefan" Institute.
§ University of Ljubljana.
|| Wageningen University.

10.1021/ci049748h CCC: $30.25
Published on Web 01/22/2005

of motion, the motional rate, as well as the polarity and proticity of the label position, resulting in several spectral components. It has to be stressed that in both lipid and protein systems, the observed heterogeneities have a long lifetime on the EPR time scale, which is about 10^{-8} s for isotropic rotational motion and is defined by the spin label interaction tensor anisotropy. This provides EPR with a unique opportunity to probe heterogeneity distributions at time scales that are important for many biochemical processes. The major stumbling block, however, is how to extract this information from the experimental EPR spectra.

To obtain biologically meaningful information from the EPR spectra, one must start with a fitting procedure, i.e., solving an inverse problem with tuning the parameters of a given biophysical model to fit the simulated spectrum with the experimental EPR spectrum. To clarify the computational demand of this problem, we would like to stress the following facts. First, one simulation of EPR spectral line shape usually includes about 20−30 spectral parameters and contains intrinsic nonlinear relations that prevent deriving the EPR line shapes analytically. It requires around 10^7 floating-point operations − 10 ms on a GigaFLOPS processor. Second, the size of the parameters' space is around $10^{20}-10^{30}$ points, if we discretize the space according to relative error of 10% of each parameter definition interval. Therefore, the optimal fitting procedure is computationally demanding. Different research groups have attempted to solve this problem by applying various self-navigating optimization methods, e.g. deterministic Downhill Simplex and Levenberg−Marquardt, stochastic Monte Carlo, or maximum-likelihood common-factor analysis.[14−19] It has to be stressed that deterministic optimization routines such as Downhill Simplex or Levenberg−Marquardt need an appropriate starting point (initial set of spectral parameters) for the optimization to converge effectively, i.e., to provide the best possible fit. Therefore, such a procedure may require time-consuming assistance of a spectroscopist (hours to days) and consequently the spectroscopist's setting of the starting parameters may bias the analysis.

Regarding the above-mentioned characteristics we approached this inverse problem solving with a stochastic population-based optimization − hybrid evolutionary optimization (HEO).[20,21] The time cost of HEO is around 10^6 simulations, which is approximately 1 h on a GigaFLOPS processor. At the same time it is not sensitive to the starting points, i.e., its effectiveness is the same when the starting population is created randomly, which consequently saves several hours or days of the spectroscopist's time.

Recently it has been proposed by Štrancar et al. that lateral heterogeneity of membranes may be described by constructing quasi-continuous distributions of EPR spectral parameters obtained from the solutions of the multiple runs of HEO.[22] However, this approach is only able to visualize the quasi-continuous distributions of EPR spectral parameters but is not able to recognize groups of related spectral components and to quantify their properties.

In this paper we continue along similar lines implementing a hybrid evolutionary optimization for EPR-based characterization of complex biosystems and introducing a novel method called GHOST to condensate solutions into groups and provide a means for a quantitative characterization of a complex biomembrane systems. The method was tested on synthetic spectra. Furthermore possible applications for lipid systems and membrane proteins are discussed. The name of the method, GHOST, was chosen after the two-dimensional ghostlike irregular shapes of groups of solutions.

COMPUTATIONAL METHODS

The majority of the present EPR spectral simulations described in the literature provides an accurate description of the spectral line shapes corresponding to different motional models of spin labels and other paramagnetic species.[16,23] Most of the simulation approaches propose different motional patterns of spin probes in a homogeneous environment and establish these models through fitting to experimental spectra of spin-labeled model systems. Thus, the heterogeneity of real biosystems is usually not taken into account. This means that the biomembrane complexity is much higher than the proposed complexity of the environment in such simulation models.

The approach to the characterization of biosystem complexity proposed in this paper is based on the *projection principle*, i.e., building the description of a complex system through collecting different projections made within a model with a finite (discrete) complexity.[22] Mathematically, this approach evolves in analogy to the expansion of the response function in a quasi-continuous space over various finite-size sets of base functions. In our case the response function and the different base functions correspond to the experimental EPR spectral line shape of the complex biomembrane system and an N_d-dimensional projection model response (simulated EPR spectral line shapes evolved as a superimposition of N_d spectral components), respectively.

From the point of view of the resolution of EPR spectroscopy, the application of the most robust and efficient optimization routines in fitting of EPR spectra enables extraction of around 20−30 spectral parameters at a time, provided the correlations between the parameters are not strong. Since usually an EPR simulation model involves 6−7 spectral parameters (see below), the 20−30 parameters correspond to approximately 4 different spectral components, that we named solutions. Note, that the term "solution" will be referred to as a subset of parameters that defines a single spectral component within one fit. The limitation to 4 solutions limits the possibilities of characterization of distributions (of parameters) in cases where the complexity of the system is very high. However, when the complexity is low, e.g. a spectrum is composed of a few sharply defined components; the extraction will be very accurate. Therefore, the use of the projection principle within a 4D-projection model (4 spectral components are allowed) and the application of multiple optimization runs, where each run can provide its own projection (approximation), can provide a possibility of characterization of the complex environments of various spin-labeled biosystems.

Therefore this approach combines the advantage of simple and fast simulation models applicable to motional patterns that are relevant at physiological temperatures for various kinds of spin-labeled biosystems, robust hybrid evolutionary optimization methods and a special data condensation algorithm.

Simulation Models. Characterization through direct modeling of a complex spin-labeled biosystem represents a highly

Table 1. Input to the Spectral Simulation Model

parameter	definition interval and units	uncertainty
S − order parameter	0−1	2%
θ − open cone angle	0−π/2	3%
ϕ − asymmetry angle of the cone	0−π/2	5%
τ_c − rotational correlation time	0.02−3 ns	6%
W − additional broadening constants	0.1−4 G (1 G = 0.1 mT)	5%
p_A − polarity correction factor on A tensor	0.8−1.2	4%
p_g − polarity correction factor on g tensor	0.9996−1.0004	6%
d − relative weight	0−1	2%

time-consuming process both from the point of view of the simulation model as well as the optimization process.

Generally, to describe the EPR spectra of spin labels, the stochastic Liouville equation is used.[16,24,25] However, in a membrane system labeled with fatty acid spin probes or a spin-labeled membrane protein or peptide, measured at physiological temperatures, the majority of the local rotational motions is fast with respect to the EPR time scale. Since the fast motion approximation is around 100 times less computational demanding, it is therefore reasonable to simplify the modeling of the spectra taken at physiological temperatures by restricting the motions to the fast motional regime.

Using multiple rotational correlation times together with multiple parameters that define the anisotropy of the rotational motions, i.e., order parameters or wobble angles, can induce numerically ill-posed optimization problem. To avoid this we decided to use a single rotational correlation time that empirically describes the rate of the rotational motion in addition to order parameters or wobble angles that define the anisotropy of the rotational motions. In some cases the model can be further simplified to depend on a single order parameter.

Since the basic approach has been already discussed elsewhere,[9,26] it is only summarized here. The model takes into account that the spectrum is composed of several spectral components reflecting different environments of the spin label and described with different sets of spectral parameters. The calculation of each spectral component involves three calculation steps. In the first step, the magnetic interaction tensors are averaged over fast stochastic restricted rotational motions of the nitroxide spin probes to calculate the resonant field distribution.[27,28] This is done by introducing an order parameter, S, or by using two angles, θ and ϕ, that define the anisotropy of rotational motion. In the same calculation step, the environmental polarity correction factors p_A and p_g are taken into account.[29] The construction of the resonant field distribution is optimized to provide a high accuracy of the directional distribution together with the fastest possible summation schemes. The second step includes the introduction of the Lorentzian line widths in the case that the motional narrowing approximation[30] is used. Two line shape parameters are applied: a rotational correlation time, τ_c, and a broadening constant W. τ_c describes the effective rate of motion, W arises primarily from unresolved hydrogen superhyperfine interactions and small contributions from minor paramagnetic impurities (e.g., due to usually present oxygen), external magnetic field inhomogeneities, and field modulation effects as well as from spin−spin interaction. Note, that the line broadening can differ among the domains due to different partitioning of spin probes, i.e., different spin label concentration, as well as different partitioning of oxygen in different membrane domains. In the third step, the convolution of the resonant field distribution with the first derivative of the line shape is calculated for all spectral lines. Special care is taken to select between FFT (fast Fourier transform) and direct methods to get the fastest convolution scheme possible for this particular problem. The proportion of a particular spectral component is taken into account according to a weighting factor d. The result of the convolution is the final line shape of the simulated EPR spectrum.

This procedure is implemented in the software package EPRSIM.[31] For the sake of clarity, we want to summarize the input parameters with the definition intervals as well as the empirically determined uncertainties of the parameters in Table 1 and stress again that output of the model is the spectral line shape y^{sim} that consist of 1024 points at the field values as defined by the experimental data of center field and field sweep. The uncertainties are defined according to the resolution of the EPR-based characterization determined via covariance-matrix analysis of the discrete problems, i.e., few-components synthetic spectra. The uncertainties represent the highest possible accuracy when resolving approximately 20−25 spectral parameters within the presented simulation model.

HEO Optimization. To guide the optimization a fitness function is introduced. It measures the goodness of fit of the simulated spectrum with the experimental one. The measure used here is the reduced χ^2, i.e., the sum of the squared residuals between the experimental and simulated spectral points (y_i^{exp} and y_i^{sim}, respectively) divided by the squared standard deviation of the experimental points σ, and by the number of points in the experimental spectrum N (in our case $N = 1024$):

$$\chi^2 = \frac{1}{N}\sum_{i=1}^{N}\frac{(y_i^{\exp} - y_i^{sim})^2}{\sigma^2} \qquad (1)$$

The standard deviation σ is assessed numerically from the points in the simulated spectrum regions where the derivatives are close to zero. This is usually at both ends of the spectrum.

Due to a complex search space of spectral parameters ($N_d = 4$, i.e., 4 groups of 6 or 7 parameters, resulting in 24 or 28 parameters), hybrid evolutionary optimization (HEO) was used as an optimization method. HEO belongs to the class of the stochastic and population based optimization algorithms. It uses a population of spectral parameter sets ("individuals"; usually 200 or 300), which are optimized at the same time.[32,33] The basic scheme of the optimization loop of the evolutionary algorithm (Figure 2) starts with the

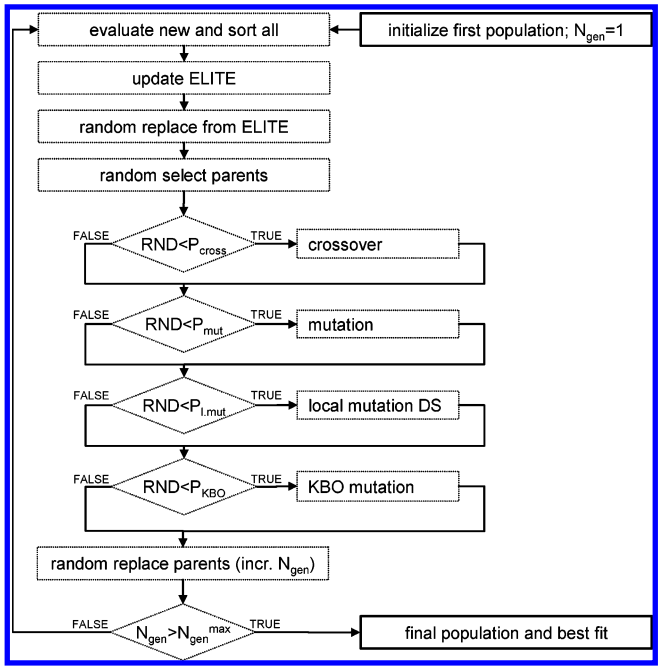

Figure 2. HEO flowchart. Schematic presentation of Hybrid Evolutionary Optimization (HEO) − a generational elitist evolutionary algorithm hybridized with stochastically called local search.

selection of parameters of some sets of spectral parameters from the population of such sets. Two types of operators are applied to generate an "offspring" population set of parameters: genetic operators and knowledge-based operators. The genetic operators comprise multipoint crossover and mutation operators as well as operator for Downhill Simplex. The knowledge-based operators are used to reduce the effect of correlation within some pairs of spectral parameters. The "offspring" population then replaces the "parent" population (generational evolutionary algorithm). To ensure that the best individual in the population (best fit to the experimental spectrum) is kept, it is also held in the "Elite". Therefore this algorithm is classified as a generational elitist evolutionary algorithm hybridized with stochastically called Downhill Simplex. Such an approach combines the benefits of the genetic algorithm and Downhill Simplex. It is successful in both finding promising regions of solutions and extracting fine-tuned solutions.[20,21] Since it is not sensitive to the starting population, this can generate randomly eliminating human input and thus enabling an automatic optimization. At the same time the stochastic nature of this optimization allows us to determine the errors in the spectral parameters independently of the covariance matrix analysis. The optimization method described is implemented in the software package EPRSIM.[31] The settings used in HEO[20,21] are summarized in Table 2.

Due to the stochastic nature of the optimization routine at least 20 HEO runs need to be executed to evaluate the results statistically. However, in a case when the proposed model complexity is lower than the complexity of the biological system and the optimization routine searches for the solutions within a projection hyperplane, the number of HEO runs M has to be increased substantially. Empirically it is found that M should be in the order of hundreds, for example 200. This results in a large amount of data, i.e., $M \times N_d$ solutions, where N_d is the number of spectral components (200 × 4 sets of 6 to 7 parameters, dependent on the model/experiment). To reduce this enormous amount of information and to quantify the characterization independently of the discrete/continuous character of the groups of solutions, we provide a novel approach, called GHOST condensation, which will be described in the next subsection.

Table 2. Settings Used in HEO Optimization

HEO parameters when using 4 spectral components	value
population size	300
elite size	2% of population size (= 6)
no. of sites for multipoint crossover	3
crossover probability	70%
mutation probability	1%
downhill simplex probability	0.2%
knowledge based operators probability	10%
no. of generations to stop optimization	100
type of selection	fitness proportional selection with linear scaling between 1 and 2 averages
type of replacement	random

GHOST Condensation. The following general tools are implemented to make the algorithm able to detect, represent, distinguish and quantify the most important groups of solutions that can be extracted and statistically approved from spin label EPR spectra.

1. Data Filtering According to the Goodness of Fit. Stochastic optimization routines that implement the usage of various random operators cannot guarantee that any fit (overall solution) found has the lowest values of $\chi 2$ even if the proposed complexity of the model is high enough to enable a satisfactory description of an experimental response. On the other hand, if the proposed complexity is too low, the phase space (space of the solutions) in which the optimization will be performed, will inherently include many global minima for $\chi 2$. Therefore, the algorithm should act in a conservative way, i.e., it should damp the (worse) solutions with the highest $\chi 2$ values and at the same time pass through those points that belong to different global minima and that do not possess the lowest $\chi 2$ due to the inappropriateness of the proposed model due to a too low complexity.

2. Data Filtering According to Local Density. The method of determining the local density of the solutions is implemented to provide a second tool to classify the quality of the solutions. In contrast to $\chi 2$ filtering, density filtering does not account for the property of a single solution (spectral component) but for a group of solutions, i.e., the solution is significant only if it can be found with higher probability, so the local density must be high enough. An important property implemented in the density calculation is the continuity of the density function across the phase space. Instead of calculating densities within a grid, or at discrete sections of the phase space, the density at a certain point in the phase space is calculated by a summation of the contributions of the tails of points spread by a Gaussian probability function, corresponding to different, not perfectly defined solutions.

3. Grouping of Solutions According to Their Neighborhood. In this part the solutions are grouped according to the neighborhood principle, defined in eq 7 in the subsection Condensation of solutions. The grouping principle reduces

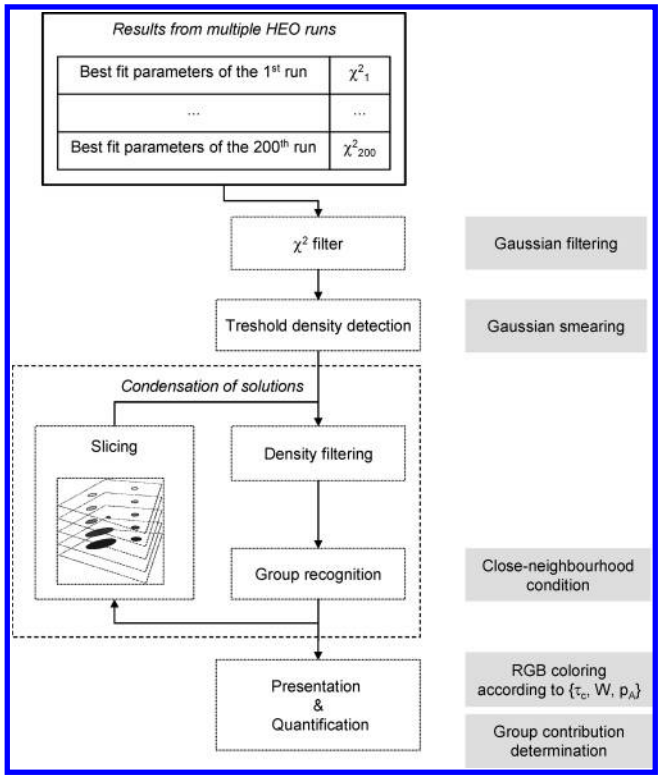

Figure 3. GHOST flowchart. Schematic presentation of the GHOST condensation method that includes filtering, grouping, and quantification of HEO best fit solutions.

the information coming out from the multiple runs of the optimization routine.

4. Quantification of the Group Contributions. The main goal of the GHOST condensation algorithm is to quantify the contributions of the groups of spectral parameters, which was found to be a nontrivial task for the following reasons. If the proposed complexity is too high, i.e., the experimental spectrum reports a low number of well-defined groups of solutions (spectral components), the contribution determined directly from the best fit of all the optimization runs seems to provide the most accurate values. If the proposed complexity is too low, i.e., the experimental spectrum includes a quasi-continuous distribution of solutions, the extraction of the contributions from best fits, that can be described as projections, is not appropriate anymore. To solve this problem, we propose that the contributions should be biased with the local solution density, i.e., the accumulated contribution of the appropriate group is obtained by summing the proportions of solutions divided by the local solution densities. In the case of a group with a high density, which one would obtain when finding a discrete group of closely spaced solutions, the calculated contribution will be close to the best-fit value. However, in the case of a low-density group, which one would obtain when finding a quasi-continuous group of distributed solutions, the contribution of the group will increase due to the accumulation of the many solutions that have not high local densities. In this way, this enables also the characterization of the quasi-continuous groups of spectral parameters.

The GHOST algorithm that includes the filtering, grouping and quantification is schematically presented in Figure 3. First, the best-fit solutions (200 best-fits from 200 optimization runs) are collected and filtered by χ^2 filtering to get a representative ensemble. Then the local density is calculated at the position of each solution in order to discard about the least significant solutions. In the following slicing procedure grouping is performed at different slice densities according to the neighborhood condition. By slicing from the highest to the lowest densities the recognition and discrimination between discrete and quasi−continuous groups of solutions is enabled. Finally, the quantification as well as parametrization of each group of solution is done. To present the resulting solutions and groups of solutions in a compact way, four different spectral parameters are used in the description of lipid domains in biomembranes: order parameter S, rotational correlation time τ_c, additional broadening W, and polarity correction factor p_A. This results in three different two-dimensional cross-section plots (S-τ_c, S-W, S-p_A) for which RGB coloring according to the normalized vector (τ_c, W, p_A) is used. In the case of the study of the low-resolution structure of membrane proteins, the order parameter is replaced by a cone angle θ and the angular amplitude of motion within a cone ϕ, respectively. In this situation an additional cross-section plot (θ-ϕ) can be presented.

Each phase of the GHOST algorithm is described in detail below.

χ^2 Filtering. Data filtering is performed according to the χ^2 of the appropriate fit using a Gaussian damping factor, which works as a low-pass filter

$$F_{\chi_i^2} = Exp\left[-(1/2)\left(\frac{\chi_i^2 - \chi_{\min}^2}{\Delta\chi^2}\right)^2\right] \qquad (2)$$

where χ^2_i is the value for χ^2 for i-th HEO run according to eq 1, χ^2_{min} is the minimum of all runs, and $\Delta\chi^2$ is the filter width. The filter width is determined such that the filter should pass through 40% of the better solutions. This number is empirically found and is based on the success rate of HEO applied on a discrete problem, which was 80%, divided by 2 to make the procedure even more stringent.

Density Calculation. The local solution density ρ_j at the position of the j-th point in the parameter space is calculated by the summation of contributions of tails of Gaussian-spread points, corresponding to different solutions positioned at the i-th points:

$$\rho_j = \sum_i Exp\left[-(1/2)\sum_k\left(\frac{p_{k,i} - p_{k,j}}{\sigma_k(d_i)}\right)^2\right] \qquad (3)$$

The summation over k represents the summation over different parameters p_k weighted by the uncertainties $\sigma_k(d_i)$ calculated as

$$\sigma_k(d_i) = \sigma_k f(d_i) \qquad (4)$$

where σ_k is the uncertainty for each parameter type k (a fraction of the appropriate definition intervals, as presented in Table 1) and $f(d_i) = 1 + d_i \exp(-d_i^2/2)$ is an empirical weighting function, which tries to correct uncertainty according to the weighting factor d_i of the particular spectral component. The form of the function $f(d_i)$ implements the idea that spectral components with smaller contributions possess larger errors in the parameters; however, spectral components with very small contributions do not represent statistically significant spectral components at all.

Density Filtering. Density filtering is implemented in two ways: within the presentation of the χ^2-equivalent solutions as well as within the condensation of solutions.

To perform density filtering and to prevent rare spectral components to influence the final characterization, a threshold density was defined to dampen the contribution of the solutions with local density lower than the threshold density. The threshold density is determined with the majority of the solutions that do not possess high values of goodness of fit, e.g. 90% of all solutions

$$\frac{\sum_{i,\rho_i > \rho_t} F_{\chi_i^2} d_i}{\sum_i F_{\chi_i^2} d_i} = 90\% \qquad (5)$$

where $F_{\chi_i^2}$ is the χ^2 filter according to eq 2, d_i is the contribution of the i-th solution, and ρ_i is the local solution density according to eq 3. The value of the threshold density is down-limited to the lowest possible threshold density ρ_t^{min}. This guarantees that at least a number, corresponding to ρ_t^{min}, of very good points (or equivalent number of points with a slightly lower χ^2) can be found in the neighborhood of each "significant" point. Usually $\rho_t^{min} = 5$ is used as the lowest possible average density in a single continuous distribution constructed with a predefined number of four spectral components and a number of HEO runs $M = 200$ resulting in 800 solution points.

Second, using the threshold density, the algorithm calculates the density filter for every point in an ensemble

$$F_{\rho_i} = Exp\left[-(1/2)\left(\frac{\rho_t}{\rho_i}\right)^2\right] \qquad (6)$$

to modify the radii for points corresponding to individual solutions in the GHOST diagram. The radius of a solution point is defined as the product of the contribution of the solution, its χ^2-filter value and the ρ-filter value. Equation 6 indicates that if the local density is much higher than the threshold density $F_{\rho_i} \rightarrow 1$, then the ρ-filter will effectively pass unperturbed solutions.

Condensation of Solutions. After the solutions are damped with the χ^2 filter and solutions with a local density lower than the threshold density are removed, the remaining set of solutions is scanned for groups of solution points.

Determination of groups of similar solution points is based on the detection of neighboring points, i.e., two points i and j are close neighbors if the following condition is fulfilled:

$$\frac{1}{N_p}\sum_k \left(\frac{p_{k,i} - p_{k,j}}{\sigma_k(d_i)}\right)^2 < 1 \qquad (7)$$

Here the summation over k represents the summation over different spectral parameters and N_p is the number of spectral parameters determining a single solution. Since the relative values of the parameters are divided with their relative uncertainties, this condition represents the condition when two solutions can be statistically indistinguishable.

To find the groups of solutions independently of their type, a special slicing procedure at different density values is implemented in the algorithm (see Figure 4a). Starting at the slice level s approaching the highest solution density ρ_i, the algorithm gives only groups of solutions that are found with high probability (high density). These are likely to be discrete-type groups of solutions, an example of which is group A in Figure 4. Continuing with slices on lower densities, different groups of points are found (Figure 4a). To confirm a particular group, it has to be found on at least two subsequent slices, i.e., the center of mass of the group on the particular slice has to fulfill the neighboring condition with the center of mass of the group on the next slice. For example, both groups A and B are found on slice levels s and $s+1$, and the average parameters on the two slices fulfill the neighboring condition. So they are both confirmed on the slice level $s+1$. Groups found on the slice level $s+2$ enable reconfirmation of the group A in addition to the detection of a new broad group. However, this broad group does not correspond to either group B (confirmed already) or group C (not confirmed), since the neighboring condition is not fulfilled neither for group B nor for group C. Because group C was not found on at least two subsequent slices it was not confirmed; the solutions comprising group C in fact belong to a broader group included in group D. On the other hand, the solutions comprising group B that was confirmed on the previous slice represent a distinguishable part of group D. The later is considered as a typical case where group B would be regarded as a discrete group superimposed on a continuous group D. Finally, on the slice level $s+3$ group A and group D are confirmed. All the confirmed groups can be presented together on a single slice as a result of the slicing procedure (Figure 4b).

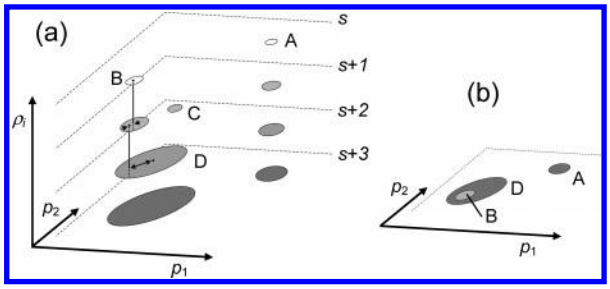

Figure 4. Slicing procedure. (a) Graphical presentation of detection procedure of discrete or quasi-continuous groups of solutions through slicing. Each slice (*s*, *s+1*, etc.) represents a two-dimensional cross-section plot of spectral parameter p_1 and spectral parameter p_2 at particular local solution density ρ_i. Capital letters A−D represent different groups of solutions that are found through slicing. The center of mass of a group of solutions is indicated with a dot, and application of the neighboring condition test on the center of mass of the groups of solutions on the two subsequent slices is indicated with arrows. (b) Single slice, with all the confirmed groups (A, B, D), that represents the result of the GHOST condensation.

Because many more solutions are needed to find continuous groups, the probability of finding them increases with decreasing the density. However, significant translations of the center of mass of a continuous group between two subsequent slices can be encountered, causing a continuous group not to be confirmed at higher density slices but at the lowest one simply because such a group usually represents large fractions of all solutions. Note that a group is rejected after slicing if its contribution falls below a predefined value σ_d.

Contribution Determination. After condensation of solutions into groups, the information (all parameters of all

solutions) is further reduced into average properties of the groups (average parameters and relative contributions). Accordingly, the contribution $d^{(n)}$ of the n-th group is determined as

$$d^{(n)} = \frac{\sum_{i \in group\ n} F_{\chi_i^2} \frac{d_i^{(n)}}{\rho_i}}{\sum_{m:all\ groups\ on\ the\ lowest\ slice} \left(\sum_{i \in group\ m} F_{\chi_i^2} \frac{d_i^{(m)}}{\rho_i} \right)} \quad (8)$$

Each other k-th parameter of the n-th group is averaged into $p_k^{(n)}*$ according to

$$p_k^{(n)*} = \frac{\sum_{i \in group\ n} F_{\chi_i^2} \frac{d_i^{(n)}}{\rho_i} p_{k,i}^{(n)}}{\sum_{i \in group\ n} F_{\chi_i^2} \frac{d_i^{(n)}}{\rho_i}} \quad (9)$$

Here $p_{k,i}^{(n)}$ is the k-th parameter of the solution i of n-th group.

To quantitatively distinguish between different types of groups, discrete or continuous group, the second moment $M_2^{(n)}$ of the n-th group of solutions is calculated according to the following equation

$$M_2^{(n)} = \sqrt{\frac{\sum_{i \in group\ n} F_{\chi_i^2} \frac{d_i^{(n)}}{\rho_i} \left(\frac{1}{N_p} \sum_k \left(\frac{p_k^{(n)*} - p_{k,i}^{(n)}}{\sigma_k} \right)^2 \right)}{\sum_{i \in group\ n} F_{\chi_i^2} \frac{d_i^{(n)}}{\rho_i}}} \quad (10)$$

It measures the width of the distribution of spectral parameters in a group of spectral solutions. For discrete groups of spectral solutions it is expected to be below or close to 1, since the distribution of the EPR spectral parameters should be in the range of the errors of the spectral parameters. For large continuous distribution of parameters it will be significantly greater than 1.

RESULTS AND DISCUSSION

To facilitate figure reading and comprehension, the results of characterization procedures will be presented in two-dimensional cross-sections as defined in the GHOST condensation subsection, where the groups of related solutions will be indicated. Two chosen parameters will be plotted on the two axes. Besides, colors will be used to represent values of the remaining spectral parameters in accordance with the RGB specifications shown in Figure 5. This provides a means for direct and easy location of the same group of solutions on different cross-section graphs. These diagrams will simply be denoted as GHOST diagrams. Particular GHOST diagrams for various combinations of two spectral parameters can be regarded as different cross-sections of the solution phase space.

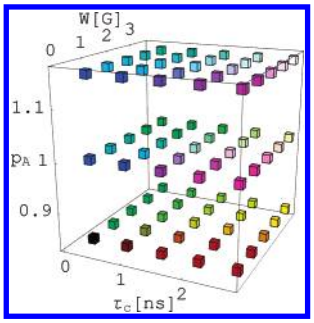

Figure 5. Color legend. The color of a solution point in a GHOST diagram is defined by the RGB specification where the intensity of each color component (red, green, and blue, respectively) represents the relative value of the spectral parameters (according to the definition intervals from Table 1).

Synthetic Spectra − Testing and Validation of the GHOST Algorithm. The first example used to validate the GHOST algorithm was a simple synthetic EPR spectrum composed of two spectral components (2D spectrum) with the original sets of spectral parameters shown in Table 3a. The spectrum was constructed within the fast motional approximation model. The synthetic spectrum was then fitted using the same model with $N_d = 4$ spectral components, i.e., in the 4-dimensional projection model (HEO 4D-projections). The average group parameters for GHOST condensation of original distribution (GHOST orig.) as well as for GHOST condensation of 4D-projections (GHOST 4D) are presented in Table 3c and Table 3b, respectively. It can be seen from comparison of Tables 3a and 3c that the GHOST condensation parameters are in a very good agreement with the original parameters used for composing synthetic EPR spectrum.

The 2D spectrum can be regarded as an example of a discrete spectrum with two well-resolved components which can be nicely resolved with the GHOST condensation (Figure 6a), although the number of components proposed in the simulation model was 4. This result indicates that the GHOST algorithm does not generate additional groups of solutions. The GHOST condensation of 4D-projections of a 2D spectrum represents an example of discrete group confirmation during the slicing process, where only groups of points with high density as well as with similar average parameters are found.

In the second example, a synthetic EPR spectrum is used that is constructed from three spectral components (see Table 4a) and fitted within the same model using four spectral components (4-D projection). The GHOST of the original distribution of spectral components of the 3D spectrum is presented in Figure 7a. Similarly as in the two-component discrete case, the positions of the groups (see e.g. S* in Tables 4b and 4c) are found with a high precision with the GHOST condensation (Figure 7b). However, the accuracy for the determination of the contributions of the three spectral components reduces to 5−10% (previously 1−2%). The group at the lowest order parameter was found with larger contribution (group index 1, Table 4c) as compared to the original one (comp. index 1, Table 4a). This is again an example of discrete group confirmation during the slicing process. However, in this case the distributions of the points are spread over a slightly wider area (the sizes of groups are lager) than in the case of a 2D spectrum (compare values of second moments of EPR spectral parameters in Table 7a

Table 3. Spectral Parameters for 2D (Discrete) Case: (a) Original Set of Spectral Parameters for Particular Spectral Components of Synthetic 2D Spectrum and Corresponding Group Parameters (b) after GHOST Condensation of Original Distribution and (c) after GHOST Condensation of HEO 4D-Projections[a]

(a) original set					(b) GHOST orig.					(c) GHOST 4D				
comp. index	S	τ_c (ns)	p_A	d (%)	group index	S^*	τ_c^* (ns)	p_A^*	d^* (%)	group index	S^*	τ_c^* (ns)	p_A^*	d^* (%)
1	0.06	1.30	0.97	40	1	0.06	1.30	0.97	40	1	0.06	1.29	0.97	41
2	0.50	0.60	1.03	60	2	0.50	0.60	1.03	60	2	0.50	0.58	1.03	59

[a] The notation of spectral parameters is the same as in Table 1. The asterisk in parts (b) and (c) denotes that an average group parameter is presented.

Table 4. Spectral Parameters for 3D (Discrete) Case: (a) Original Set of Spectral Parameters for Particular Spectral Components of Synthetic 3D Spectrum and Corresponding Group Parameters (b) after GHOST Condensation of Original Distribution and (c) after GHOST Condensation of HEO 4D-Projections[a]

(a) original set					(b) GHOST orig.					(c) GHOST 4D				
comp. index	S	τ_c (ns)	p_A	d (%)	group index	S^*	τ_c^* (ns)	p_A^*	d^* (%)	group index	S^*	τ_c^* (ns)	p_A^*	d^* (%)
1	0.06	1.30	0.97	28	1	0.06	1.30	0.97	28	1	0.08	1.34	0.96	37
2	0.22	1.10	1.00	30	2	0.22	1.10	1.00	30	2	0.22	1.13	1.01	25
3	0.50	0.60	1.03	42	3	0.50	0.60	1.03	42	3	0.50	0.57	1.03	37

[a] The notation as in Table 3.

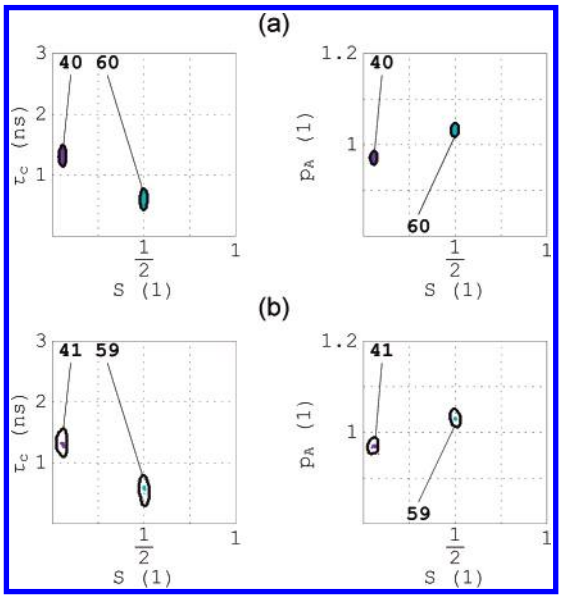

Figure 6. 2D (discrete) case. Distributions of spectral parameters of the EPR spectrum originally made of two spectral components. (a) The result of GHOST condensation of original distribution of spectral components composing the synthetic spectrum. (b) The result of GHOST condensation of distribution of solutions constructed from HEO 4D-projections.

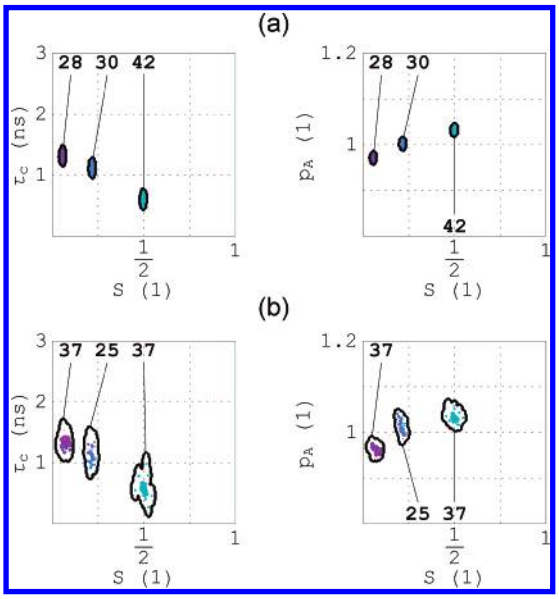

Figure 7. 3D (discrete) case. Distributions of spectral parameters of the EPR spectrum originally made of three spectral components. (a) The result of GHOST condensation of original distribution of spectral components composing the synthetic spectrum. (b) The result of GHOST condensation of distribution of solutions constructed from HEO 4D-projections.

and 7b), simply because there were more parameters to resolve. Note that the spreading of the parameters in this case is close to the uncertainties defined in Table 1.

The third example shows a synthetic EPR spectrum with 15 spectral components. In this spectrum, two spectral components were constructed with significantly higher contribution relative to the others (see Table 5a). This 2+13D spectrum is an example of a combined discrete and quasi-continuous spectrum. Such an example cannot be directly fitted within an existing model, because the number of spectral components within the simulation model is limited to 4. It also cannot be extracted directly through modification of the model, since such a model would need too many parameters (89 parameters), thereby exceeding the EPR resolution limit. The GHOST condensation of the original distribution already shows some averaging: from the 15 spectral components 4 separate groups were generated (Table 5b and Figure 8a). This arises because some of the groups of original points are close to each other and fulfill the neighboring condition of eq 7. Moreover, the GHOST condensation of 4D-projections gives an even more continuous picture; it detects the presence of two large groups of solutions on the lowest slice (Table 5c and Figure 8b), covering the positions of all the spectral component points.

Another feature can be seen in the GHOST diagram of 4D-projections of the 2+13D spectrum (Figure 8b). Within the group (at the lowest slice) at low order parameter another group of solutions with higher density (at the higher slices) is present (see Figure 8b), which is the consequence of the presence of a spectral component with a high proportion in the original distribution (comp. index 1, Table 5a). This spectral component with a contribution of 20% is merged

Table 5. Spectral Parameters for 2+13D (Discrete + Quasi-Continuous) Case: (a) Original Set of Spectral Parameters for Particular Spectral Components of Synthetic 2+13D Spectrum and Corresponding Group Parameters (b) after GHOST Condensation of Original Distribution and (c) after GHOST Condensation of HEO 4D-Projections (*Lowest Slice Only*)[a]

(a) original set					(b) GHOST orig.					(c) GHOST 4D				
comp. index	S	τ_c (ns)	p_A	d (%)	group index	S*	τ_c* (ns)	p_A*	d* (%)	group index	S*	τ_c* (ns)	p_A*	d* (%)
1	0.06	1.30	0.97	20	1	0.10	1.25	0.98	38	1	0.19	1.31	0.99	58
2	0.10	1.20	1.00	5										
3	0.13	1.23	1.00	4										
4	0.16	1.15	1.00	5										
5	0.20	1.20	1.00	4										
6	0.30	1.00	1.00	3	2	0.34	1.06	1.01	23					
7	0.30	1.12	1.00	4										
8	0.32	1.18	1.00	3										
9	0.32	1.08	1.00	4										
10	0.37	0.95	1.03	3										
11	0.38	1.08	1.03	3										
12	0.40	0.95	1.03	3										
13	0.50	0.60	1.03	30	3	0.51	0.64	1.03	34	2	0.50	0.73	1.03	42
14	0.55	0.90	1.03	4										
15	0.62	1.40	1.10	5	4	0.62	1.40	1.10	5					

[a] The notation as in Table 3.

Table 6. Spectral Parameters for 15D (Quasi-Continuous) Case: (a) Original Set of Spectral Parameters for Particular Spectral Components of Synthetic 15D Spectrum and Corresponding Group Parameters (b) after GHOST Condensation of Original Distribution and (c) after GHOST Condensation of HEO 4D-Projections (*Lowest Slice Only*)[a]

(a) original set					(b) GHOST orig.					(c) GHOST 4D				
comp. index	S	τ_c (ns)	p_A	d (%)	group index	S*	τ_c* (ns)	p_A*	d* (%)	group index	S*	τ_c* (ns)	p_A*	d* (%)
1	0.15	1.00	1.08	6.66	1	0.36	1.00	1.01	100	1	0.35	1.17	1.01	100
2	0.18	1.00	1.07	6.66										
3	0.21	1.00	1.06	6.66										
4	0.24	1.00	1.05	6.66										
5	0.27	1.00	1.04	6.66										
6	0.30	1.00	1.03	6.66										
7	0.33	1.00	1.02	6.66										
8	0.36	1.00	1.01	6.66										
9	0.39	1.00	1.00	6.66										
10	0.42	1.00	0.99	6.66										
11	0.45	1.00	0.98	6.66										
12	0.48	1.00	0.97	6.66										
13	0.51	1.00	0.96	6.66										
14	0.54	1.00	0.95	6.66										
15	0.57	1.00	0.94	6.66										

[a] The notation as in Table 3.

Table 7. Second Moments M_2, Calculated According to Eq 10, of EPR Spectral Parameters of Groups of Solutions Found by GHOST Condensation of HEO 4D-Projections on Different Density Slice Levels for (a) 2D Spectrum, (b) 3D Spectrum, (c) 2+13D Spectrum, and (d) 15D Spectrum

	group index	slice level	M_2
(a) 2D	1	lowest	0.2
	2	lowest	0.3
(b) 3D	1	lowest	1.0
	2	lowest	1.7
	3	lowest	1.3
(c) 2+13D	1	lowest	3.3
	2	lowest	2.1
	3	higher	1.9
(d) 15D	1	lowest	4.5
	2	higher	2.5
	3	higher	2.1

with small neighboring spectral components (components 2−5, Table 5a) into one group (group index 1, Table 5b) in the GHOST condensation of the original distribution. In the GHOST condensation of the 4D-projections the corresponding discrete group is found with a contribution of 24% (originally 20%) at a higher slice (Figure 8b) but merged with several solutions with lower density to give a continuous group with a contribution of 58% at the lowest slice (group index 1, Table 5c; originally 61%). Accordingly, the slicing process of this group of points obviously results in a discrete group superimposed on a continuous group. The group with a contribution of 42% (group index 2, Table 5c) is also found on the lowest slice, but the distribution of the points is not so wide (originally this should be a discrete group of 30% superimposed on 9% background). This can be seen from Table 7c, by comparing the second moment for group 1 and 2. The character of group 2 seems to be closer to a discrete than a continuous character. Thus, in this example of a 2+13D EPR spectrum composed of a quasi-continuous and two discrete spectral components, both discrete components and one continuous group were found in the GHOST condensation procedure.

The fourth example consists of a quasi-continuous synthetic spectrum, composed of 15 spectral components of equal fractions that are given in Table 6a. This represents an extreme situation, which is used to test the limits of the GHOST algorithm. On the contrary to the previous examples

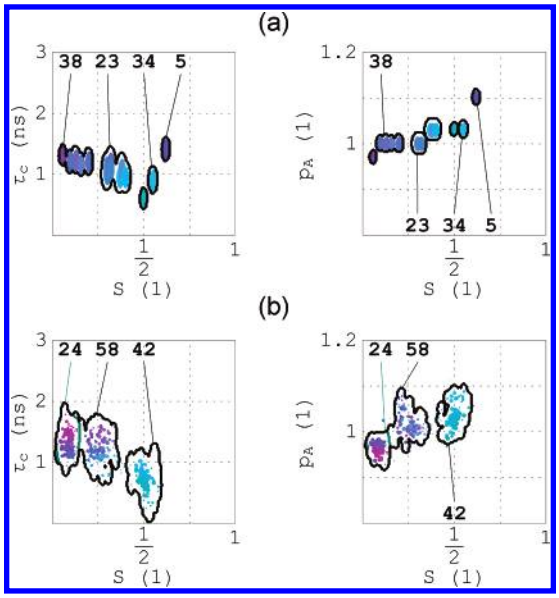

Figure 8. 2+13D (discrete + quasi-continuous) case. Distributions of spectral parameters of the EPR spectrum originally made of two discrete spectral components with high relative proportions and of 13 minor spectral components. (a) The result of GHOST condensation of original distribution of spectral components composing the synthetic spectrum. (b) The result of GHOST condensation of distribution of solutions constructed from HEO 4D-projections.

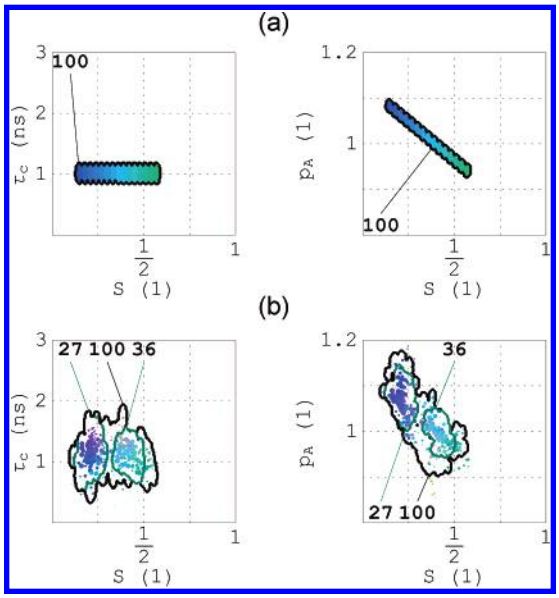

Figure 9. 15D (quasi-continuous) case. Distributions of spectral parameters of the EPR spectrum originally made of 15 spectral components with equal relative proportions mimicking continuous distribution of parameters. (a) The result of GHOST condensation of original distribution of spectral components composing the synthetic spectrum. (b) The result of GHOST condensation of distribution of solutions constructed from HEO 4D-projections.

this spectrum does not have any major spectral components with high fraction. Therefore, the characterization of this example needs a special approach such as GHOST to be determined. The GHOST condensation of the original distribution merges all the solutions into one group (Figure 9a, Table 6b). The GHOST of the 4D-projections also finds one group (Figure 9b, Table 6c). In addition, intervals of all spectral parameters are detected (Figure 9b), showing that the GHOST condensation procedure is useful in resolving continuous distributions of parameters. Especially the intervals for the order parameter (compare Figures 9a and 9b) are recognized quite accurately, since the group expands approximately from order parameter 0.15 to 0.6. On the other hand, the group shows larger intervals for the polarity correction factor (compare S-p_A diagrams in Figures 9a and 9b) and even larger for the rotational correlation time (compare S-τ_c diagrams in Figures 9a and 9b) as compared to the GHOST diagram of the original distribution. These observations are in agreement with our previous empirical finding that the goodness of fit of an EPR spectrum is the most sensitive to the order parameter and the least sensitive to the rotational correlation time.[9] It also confirms the proposed uncertainties of individual parameters as defined in Table 1.

The group found on the lowest slice is typical for a continuous group. First, the solutions are found on a low-density slice. And second, it is recognized by its large contribution, in this case 100%, as well as by the property that the distribution of spectral parameters is wide. This is also reflected by the second moment of group 1 in Table 7d. In addition to the continuous group, two groups of solutions are found at a higher slice level of the density of solutions (Figure 9b) even though the spectral components in the original distribution have the same fractions (Table 6a). This originates in the property of the EPR spectrum, which is more sensitive to variations at lower and at higher order parameters but less sensitive to variations at intermediate order parameters. Therefore, on one hand the results of GHOST condensation of the 15D spectrum proves it is capable of resolving quasi-continuous distribution, but, on the other hand, the presence of groups on the higher density slice shows that the method is limited in accurately characterizing such an extreme case. According to Table 7 one can see that discrete groups of solutions have second moment values in the interval $0 < M_2 < 2$ in the case of synthetic spectra, while M_2 values of quasi-continuous distributions have values of the second moment above 2. Therefore the second moment is a useful tool to distinguish between discrete groups of solutions and continuously distributed ones.

GHOST Applications for Membranes and Protein Structures. It is generally accepted that the membrane fluidity of proliferative cancer cells increases with the cell density, whereas the membrane fluidity of normal cell is not influenced by cell density.[34] The increased membrane fluidity of tumor cells as compared to normal tissue is reflected in the EPR spectra of spin-labeled cells through larger contributions of spectral components with a low order parameter.[35] Distinct chemical changes in the glycolipids and glycoproteins are known to occur in malignant transformation of cells[36] and a clustering of saccharide-binding sites was proposed based on the fluid mosaic model.[37] It was also suggested that the biological function of membrane fluidity is to permit some critical integral proteins to retain their translational mobility in the plane of the membrane, as an obligatory step in their function.[37] In the application of the GHOST condensation discussed here, our purpose is to show that not only the membrane fluidity changes but also the number and properties (other than the fractions) of the different membrane domains change according to the cell density of transformed cells. This information can be conveniently obtained with the GHOST condensation of

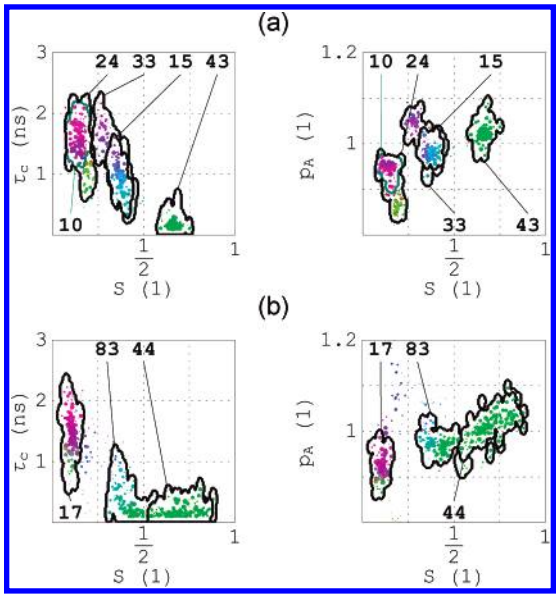

Figure 10. Example of GHOST condensation of MT1 breast cancer cells. Distributions of solutions of the EPR spectrum of MEFASL (10,3) spin labeled MT1 breast cancer cells. (a) Cells growing 3 days at $(3.9\pm0.4)*10^6$ cells in the culture flask. (b) Cells growing 5 days at $(10.4\pm1.8)*10^6$ cells in the culture flask.

solutions, since the number and properties of the different groups of solutions is detected automatically.

MT1 breast cancer cells were seeded at approximately 10^6 cells in a culture flask with surface area of 75 cm^2. EPR spectra of cell membranes spin labeled with the methyl ester of 5-doxyl palmitate, MeFASL(10,3), were measured for several days. The GHOST profiles for day 3 at a cell density of $(3.9\pm0.4) \times 10^6$ cells in the culture flask and day 5 at a cell density of $(10.4\pm1.8) \times 10^6$ per culture flask are shown in Figures 10a and 10b, respectively. In Figure 10, it can be seen that the membrane domain structure of the cancer cells is altered, as is indicated by a change in the relative fractions of the spectral components. At a low cell density, when the cell number increases at the highest rate and all the cells grow in one layer on the bottom of the flask, two additional groups of solutions are revealed (Figure 10a), which are not present at higher cell densities (Figure 10b). EPR spectroscopy cannot determine the function of these groups of solutions, but it can detect the presence of certain groups in the early stages of cell culture growth. This suggests that not only the cell membrane fluidity, as given by the relative fraction of spectral components with a low order parameter, but also other properties of the membrane heterogeneity might play an important role in the physiology of the cells.

Another important application of the GHOST condensation approach foreseen in the future is the study of protein structures by site-directed spin labeling (SDSL) EPR. Proteins are intrinsically flexible structures that can exist in multiple conformations. If conformers have similar energies, multiple states may be thermally populated at equilibrium. Although conformational transitions are very important, because they mediate protein function, it is experimentally extremely difficult to measure them. With its appropriate time scale for protein conformational rearrangements, SDSL EPR is emerging as a powerful technique for exploring structure and dynamics of both water-soluble and membrane proteins.[38] In this study we have used the membrane-bound form of the major coat protein of bacteriophage M13 as a well-documented model system.[39] For the purpose of SDSL the amino acid residues at either position 34 or 49 were replaced by a cysteine and spin labeled with the 3-maleimide-proxyl spin label. Labeled proteins were reconstituted in DOPC lipid bilayers and EPR spectra were recorded.[12] For this case, two angles that describe the restrictions of rotational motion are used in the EPR simulation model. The first angle, θ, corresponds to the opening angle of the "free-space" cone

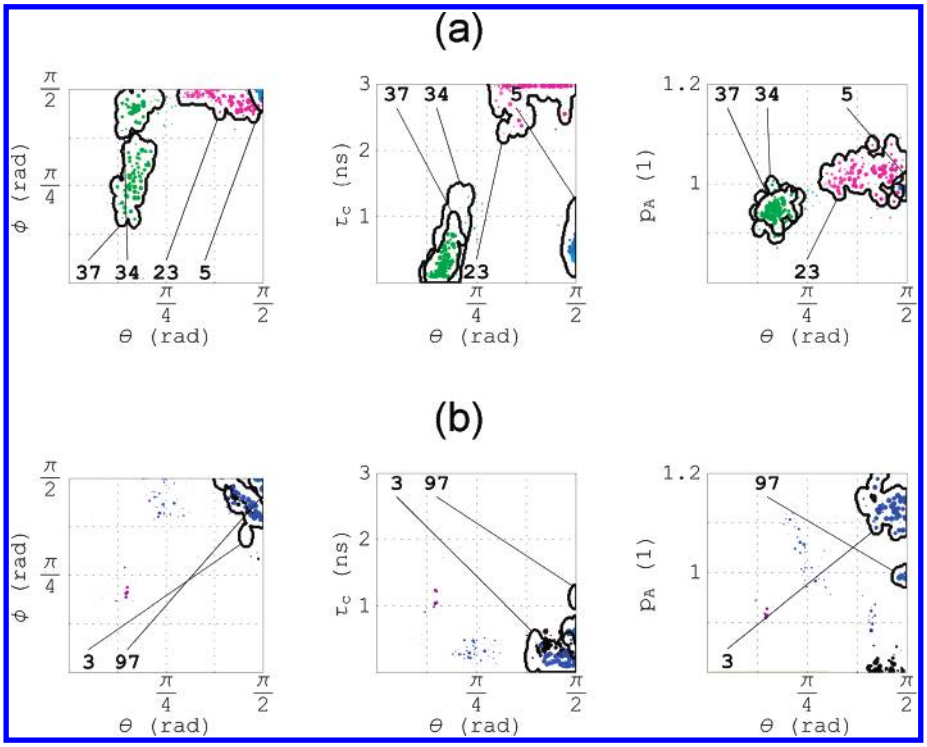

Figure 11. Example of GHOST condensation of SDSL-EPR of M13 coat protein. (a) EPR spectrum of spin labeled position 34. (b) EPR spectrum of spin labeled position 49.

of the spin label, and the second angle, ϕ, represents the anisotropy of this cone.

The two labeled sites on the major coat protein were selected to represent a water-accessible site (position 49) and position on the protein near the center of the lipid bilayer (position 34).[12,40] The different sensitivity to rotational motional restriction of the two labeled sites can be nicely observed from the GHOST condensation data (Figure 11). In the case of labeled position 34 (Figure 11a), there are at least three conformations with a different degree of restricted rotational motion. The boundaries between the different groups are not well defined. This new information arising from the GHOST condensation approach suggests the existence of multiple conformations at the labeled site of the protein. On the other hand, in the case of labeled position 49 (Figure 11b) there are only isotropic groups of solutions present with almost no restriction on rotational motion. This is consistent with a unstructured random coil conformation of the C terminus of the protein, as suggested also by high-resolution NMR.[41] From a comparison of the GHOSTs of the two labeled sites one can additionally find out that some nonspecific labeling is present (Figure 11a). This is recognized by the blue (fast) group at the location of no rotational restriction at all. This kind of information could be gained without any prior knowledge of the system, especially without the knowledge of how many and what kind of conformations exist in the case of membrane protein or peptide. This illustrates another advantage of the GHOST algorithm. Therefore, the GHOST data in turn give conformational, polarity and rotational correlation distributions that would otherwise not be available.

In conclusion, the two experimental examples show that by using the novel GHOST condensation method, the enormous volume of information obtained from multiple HEO runs can be successfully reduced to provide the average properties of the groups of different solutions at an appropriate complexity. The method is able to automatically detect the degree of biosystem complexity and therefore has a high potential for biological applications.

ACKNOWLEDGMENT

This work was carried out with the financial support of the Ministry of Education, Science and Sport of the Republic of Slovenia. Initiation of the collaboration between the authors was enabled by the financial support from EC COST D22 Action.

REFERENCES AND NOTES

(1) Bloom, M.; Thewalt, J. L. Time and distance scales of membrane domain organization. *Mol. Membr. Biol.* **1995**, *12*, 9−13.

(2) Edidin, M. Lipid microdomains in cell surface membranes. *Curr. Opin. Struct. Biol.* **1997**, *7*, 528−532.

(3) Maxfield, F. R. Plasma membrane microdomains. *Curr. Opin. Cell Biol.* **2002**, *14*, 483−487.

(4) Jørgensen, K.; Mouritsen, O. G. Phase Separation Dynamics and Lateral Organization of Two-Component Lipid Membranes. *Biophys. J.* **1995**, *69*, 942−954.

(5) Leidy, C.; Wolkers, W. F.; Jørgensen, K.; Mouritsen, O. G.; Crowe, J. H. Lateral Organization and Domain Formation in a Two-Component Lipid Membrane System. *Biophys. J.* **2001**, *80*, 1819−1828.

(6) Koklič, T.; Šentjurc, M.; Zeisig, R. The Influence of Cholesterol and Charge on the Membrane Domains of Alkylphospholipid Liposomes as Studied by EPR. *J. Lipos. Res.* **2002**, *12*, 335−352.

(7) Marsh, D.; Horvath, L. I. Structure, dynamics and composition of the lipid−protein interface. Perspectives from spin-labeling. *Biochim. Biophys. Acta* **1998**, *1376*, 267−296.

(8) Ge, M.; Gidwani, A.; Brown, A.; Holowka, D.; Baird, B.; Freed, J. H. Ordered and Disordered Phases Coexist in Plasma Membrane Vesicles of RBL-2H3 Mast Cells. An ESR Study. *Biophys. J.* **2003**, *85*, 1278−1288.

(9) Štrancar, J.; Šentjurc, M.; Schara, M. Fast and accurate characterization of biological membranes by EPR spectral simulations of nitroxides. *J. Magn. Reson.* **2000**, *142*, 254−265.

(10) Arsov, Z.; Schara, M.; Štrancar, J. Quantifying the Lateral Lipid Domain Properties in Erythrocyte Ghost Membranes Using EPR−Spectra Decomposition. *J. Magn. Reson.* **2002**, *157*, 52−60.

(11) Steinhoff, H. J.; Hubbell, W. L. Calculation of Electron Paramagnetic Resonance Spectra from Brownian Dynamics Trajectories: Application to Nitroxide Sice Chains in Proteins. *Biophys. J.* **1996**, *71*, 2201−2212.

(12) Stopar, D.; Jansen, K. A. J.; Páli, T.; Marsh, D.; Hemminga, M. A. Membrane location of spin-labeled M13 major coat protein mutants determined by paramagnetic relaxation agents. *Biochemistry* **1997**, *36*, 8261−8268.

(13) Columbus, L.; Hubbell, W. L. A new spin on protein dynamics. *Trends Biochem. Sci.* **2002**, *27*, 288−295.

(14) Kirste, B. Methods for automated analysis and simulation of electron paramagnetic resonance spectra. *Anal. Chim. Acta* **1992**, *265*, 191−200.

(15) Chachaty, C.; Soulie, E. J. Determination of Electron Spin Resonance Static and Dynamic Parameters by Automated Fitting of the Spectra. *J. Phys. III* **1995**, *5*, 1927−1952.

(16) Budil, D. E.; Lee, S.; Saxena, S.; Freed, J. H. Nonlinear-Least-Squares Analysis of Slow-Motion EPR Spectra in One and Two Dimensions Using a Modified Levenberg−Marquardt Algorithm. *J. Magn. Reson. A* **1996**, *120*, 155−189.

(17) Eviatar, H.; van der Heide, U. A.; Levine, Y. K. Computer simulations of the electron spin resonance spectra of steroid and fatty acid nitroxide probes in bilayer systems. *J. Chem. Phys.* **1995**, *102*, 3135−3145.

(18) Della Lunga, G.; Pogni, R.; Basosi, R. Global versus local minimization procedures for the determination of spin Hamiltonian parameters from electron spin resonance spectra. *Mol. Phys.* **1998**, *95*, 1275−1281.

(19) Moens, P.; De Volder, P.; Hoogewijs, R.; Callens, F.; Verbeeck, R. Maximum-Likelihood Common-Factor Analysis as a Powerful Tool in Decomposing Multicomponent EPR Powder Spectra. *J. Magn. Reson.* A **1993**, *101*, 1−15.

(20) Filipič, B.; Štrancar, J. Tuning EPR spectral parameters with a genetic algorithm. *Appl. Soft Comput.* **2001**, *1*, 83−90.

(21) Filipič, B.; Štrancar, J. Evolutionary Computational Support for the Characterization of Biological Systems. In *Evolutionary Computation in Bioinformatics*; Fogel, G. B., Corne D. W., Eds.; Morgan Kaufmann Publishers: San Francisco, 2002; pp 279−294.

(22) Štrancar, J.; Koklič, T.; Arsov, Z. Soft Picture of Lateral Heterogeneity in Biomembranes. *J. Membr. Biol.* **2003**, 196, 135−146.

(23) Meirovitch, E.; Nayeem, A.; Freed, J. H. Analysis of Protein−Lipid Interactions Based on Model Simulations of Electron Spin Resonance Spectra. *J. Phys. Chem.* **1984**, *88*, 3454−3465.

(24) Robinson, B.; Thomann, H.; Beth, A.; Fayer, P.; Dalton, L. R. The phenomenon of magnetic resonance: Theoretical considerations. In *EPR and Advanced EPR Studies of Biological Systems*; Dalton, L. R., Ed.; CRC Press: Boca Raton, 1985; pp 11−110.

(25) Schneider, D. J.; Freed, J. H. Calculating Slow Motional Magnetic Resonance Spectra: A User's Guide. In *Biological Magnetic Resonance: Spin Labeling, Theory and Applications*; Berliner, L. J., Reuben, J., Eds.; Plenum Press: New York, 1989; pp 1−76.

(26) Schindler, H.; Seelig, J. EPR spectra of spin labels in lipid bilayers. *J. Chem. Phys.* **1973**, 59, 1841−1850.

(27) Van, S. P.; Birrell, G. B.; Griffith, O. H. Rapid anisotropic motion of spin labels: Models for motion averaging of the ESR parameters. *J. Magn. Reson.* **1974**, *15*, 444−459.

(28) Griffith, O. H.; Jost, P. C. Lipid Spin Labels in Biological Membranes. In *Spin Labeling, Theory and Application*; Berliner, L. J., Ed.; Academic Press: New York, 1976; pp 453−523.

(29) Marsh, D. Electron Spin Resonance: Spin Labels. In *Membrane Spectroscopy*; Grell, E., Ed.; Springer-Verlag: Berlin, 1981; pp 51−142.

(30) Nordio, P. L. General magnetic resonance theory. In *Spin Labeling, Theory and Application*; Berliner, L. J., Ed.; Academic Press: New York, 1976; pp 5−51.

(31) Štrancar, J. EPRSIM Version 5.7. Janez Štrancar, 1996−2004, http://www.ijs.si/ijs/dept/epr/index.html.

(32) Goldberg, D. E. *Genetic Algorithms in Search, Optimization and Machine Learning*; Addison-Wesley: Reading, 1989.

(33) Eiben, A. E.; Smith, J. E. *Introduction to Evolutionary Computing*; Springer-Verlag: Berlin, 2003.

(34) Shinitzky, M. Membrane fluidity and cellular functions. In *Physiology of Membrane Fluidity Vol. 1*; Shinitzky, M., Ed.; CRC Press: Boca Raton, 1984; pp 1−51.
(35) Sok, M.; Šentjurc, M.; Schara, M. Membrane fluidity characteristics of human lung cancer. *Cancer Lett.* **1999**, *139*, 215−220.
(36) Buck, C. A.; Glick, M. C.; Warren, L. A comparative study of glycoproteins from the surface of control and Rous sarcoma virus transformed hamster cells. *Biochemistry* **1970**, *9*, 4567−4576.
(37) Singer, S. J.; Nicolson, G. L. The fluid mosaic model of the structure of cell membranes. *Science* **1972**, *175*, 720−731.
(38) Mchaourab, H. S.; Oh, K. J.; Fang, C. J.; Hubbell, W. L. Conformation of T4 lysozyme in solution. Hinge-bending motion and the substrate-induced conformational transition studied by site-directed spin labeling. *Biochemistry* **1997**, *36*, 307−316.
(39) Stopar, D.; Spruijt, R. B.; Wolfs, C. J. A. M.; Hemminga, M. A. Protein−lipid interactions of bacteriophage M13 major coat protein. *Biochim. Biophys. Acta* **2003**, *1611*, 5−15.
(40) Spruijt, R. B.; Wolfs, C. J. A. M.; Verver, J. W. G.; Hemminga, M. A. Accessibility and environmental probing using cysteine residues introduced along the putative transmembrane domain of the major coat protein of bacteriophage M13. *Biochemistry* **1996**, *35*, 10383−10391.
(41) Papavoine, C. H. M.; Christiaans, B. E. C.; Folmer, R. H. A.; Konings, R. N. H.; Hilbers, C. W. Solution structure of the M13 major coat protein in detergent micelles: a basis for model of phage assembly involving specific residues. *J. Mol. Biol.* **1998**, *282*, 401−419.

CI049748H